

Feedbacks of sedimentation on crustal heat flow: New insights from the Vøring Basin, Norwegian Sea

S. Theissen and L. H. Rüpke

The Future Ocean, IFM-GEOMAR, Leibniz Institute of Marine Sciences (at Kiel University), Kiel, Germany

ABSTRACT

Basement heat flow is one of the key unknowns in sedimentary basin analysis. Its quantification is challenging not in the least due to the various feedback mechanisms between the basin and lithosphere processes. This study explores two main feedbacks, sediment blanketing and thinning of sediments during lithospheric stretching, in a series of synthetic models and a reconstruction case study from the Norwegian Sea. Three types of basin models are used: (1) a newly developed one-dimensional (1D) forward model, (2) a decompaction/backstripping approach and (3) the commercial basin modelling software TECMOD2D for automated forward basin reconstructions. The blanketing effect of sedimentation is reviewed and systematically studied in a suite of 1D model runs. We find that even for moderate sedimentation rates (0.5 mm year^{-1}), basement heat flow is depressed by $\sim 25\%$ with respect to the case without sedimentation; for high sedimentation rates (1.5 mm year^{-1}), basement heat flow is depressed by $\sim 50\%$. We have further compared different methods for computing sedimentation rates from the presently observed stratigraphy. Here, we find that decompaction/backstripping-based methods may systematically underestimate sedimentation rates and total subsidence. The reason for this is that sediments are thinned during lithosphere extension in forward basin models while there are not in backstripping/decompaction approaches. The importance of sediment blanketing and differences in modelling approaches is illustrated in a reconstruction case study from the Norwegian Sea. The thermal and structural evolution of a transect across the Vøring Basin has been reconstructed using the backstripping/decompaction approach and TECMOD2D. Computed total subsidence curves differ by up to $\sim 3 \text{ km}$ and differences in computed basement heat flows reach up to 50% . These findings show that strong feedbacks exist between basin and lithosphere processes and that resolving them require integrated lithosphere-scale basin models.

INTRODUCTION

Information on the nature and origin of rift basins is preserved in the presently observed stratigraphy at sedimentary basins and passive margins. The key geological processes leading to basin formation like active syn-rift tectonics, post-rift subsidence, sediment and water loading all leave their characteristic fingerprints in the stratigraphic record. Basin modelling aims at recovering this information from the stratigraphy observed with the goal of gaining a quantitative understanding of a basin's structural and thermal evolution. Suggested basin reconstruction approaches can be categorised into reverse and forward models. The classic backstripping-decompaction approach (Steckler & Watts, 1978; Watts *et al.*, 1982) is an example of reverse modelling. The subsidence history is recovered by the consecutive decompaction of individual sedimentary packages using the present configuration as a starting point. Forward models start with the pre-rift

configuration and resolve basin formation forward in time (Kooi *et al.*, 1992; Kusznir & Ziegler, 1992; White, 1993). Both methods have their strengths and limitations; backstripping allows for very good data integration but the thermal and structural solutions need to be computed separately. Forward models provide coupled solutions and account for all feedbacks but are more complex and data integration more challenging. Choosing the best reconstruction approach requires detailed knowledge of the various feedbacks between the structural and thermal solutions as well as between basin and lithosphere-scale processes. One key feedback mechanism is the blanketing effect of sedimentation. It is well known that high sedimentation rates can depress basement heat flow (Debrèmaecker, 1983; Zhang, 1993; Tervoerde & Bertotti, 1994). Quantifying this effect requires information on sedimentation rates through time. Different methods for the calculation of sedimentation rates have been suggested: compacted sedimentation rates can be computed by simply taking the present thicknesses of individual sediment packages and dividing them by their age spans. Decompaction methods can be used to compute more realistic uncompacted sedimentation rates. Forward basin models

Correspondence: S. Theissen, The Future Ocean, IFM-GEOMAR, Leibniz Institute of Marine Sciences (at Kiel University), Wischhofstr. 1-3, 24148 Kiel, Germany. E-mail: stheissen@ifm-geomar.de

resolve sedimentation and compaction processes and automatically provide uncompacted sedimentation rates through time. A key question is if the basement–sediment interface is a major detachment zone; if it is, sediment thicknesses are unaffected by crustal thinning; if not, and this is in our view the more realistic case, sediment thicknesses have to be adjusted for crustal thinning. In the latter case, decompaction methods will systematically underestimate sedimentation rates. In fact, Wangen & Faleide (2008) have recently pointed out how this effect can be included in reverse basin models. Forward models do typically account for stretching-induced sediment thinning and may therefore provide more accurate and typically higher sedimentation rates through time. Determining the correct rates is essential for assessing possible feedbacks between basin and lithosphere processes like the mentioned blanketing effect. In this paper, we will first review the physics of sediment blanketing before quantifying the importance of it in a case study. In this case study, we have reconstructed the structural and thermal evolution of the Vøring Basin in the Norwegian Sea using both the classic decompaction-backstripping method and a fully coupled forward modelling approach. This comparison demonstrates the importance of accounting for the feedbacks between basin and lithosphere processes by illustrating how computed sedimentation rates differ between both approaches and how these differences feed back into the computed thermal and structural solutions.

BASIN-MODELLING APPROACHES

The feedbacks of sedimentation on crustal heat flow are studied with two different basin-modelling approaches. The first one is a forward lithosphere-scale basin-modelling approach similar to the one presented by Rupke *et al.* (2008). The second one is the classic decompaction/backstripping analysis. We will briefly describe both methods before applying them in synthetic models and in the reconstruction case study of the Vøring Basin.

Forward modelling

In this study, we use two different implementations of the general forward basin modelling approach described by Rupke *et al.* (2008). The first implementation is a newly developed one-dimensional (1D) basin model tailored for exploring the physics of sediment blanketing. This model resolves for thinning, local airy isostasy, heat transfer, sedimentation and compaction on a Lagrangian finite-element mesh. Heat transfer is assumed to occur by advection and diffusion

$$\rho c_p \left(\frac{\partial T}{\partial t} + v_z \frac{\partial T}{\partial z} \right) = \frac{\partial}{\partial z} \left(k \frac{\partial T}{\partial z} \right) + Q \quad (1)$$

where ρ , c_p , k , T , t , z , v_z and Q are density, specific heat, thermal conductivity, temperature, time, space coordinate, advection velocity and radiogenic heat generation, respec-

tively. All material properties can be variable. The diffusion part of Eqn. (1) is solved using the finite-element method. The advection part of Eqn. (1) is accounted for by deforming the mesh with the pure shear velocities

$$v_z = -\Delta z \dot{\epsilon}_z = -\frac{\Delta z \ln(\beta)}{\Delta t} \quad (2)$$

where Δz is the distance from the necking level (set to the top of the basement) and β is the local stretching factor for the current time step. The temperatures are, therefore, updated with the deforming mesh and Eqn. (1) simplifies to the diffusion equation

$$\rho c_p \frac{\partial T}{\partial t} = \frac{\partial}{\partial z} \left(k \frac{\partial T}{\partial z} \right) + Q \quad (3)$$

The Lagrangian mesh is further deformed during sedimentation and compaction. For every time step, a new sediment package is deposited and its upper boundary becomes a new mesh point. The thickness of the new sediment package is controlled by the available accommodation space, the assumed water depth for the current time step and a limiter on sedimentation rate. If accommodation space is available, the upper boundary of the new sediment package is set to the minimum of (1) the assumed water depth for the current time step and (2) the old sediment surface plus the sedimentation rate times the time step. During every time step, old sediments are compacted using a depth-dependent porosity function (Athy, 1930; Selater & Christie, 1980)

$$\phi = \phi_0 e^{(-cz)} \quad (4)$$

where ϕ , ϕ_0 and c are the porosity, surface porosity and compaction length scale. The latter two are material properties that can vary. The porosity in Eqn. (4) feeds back into the heat transfer Eqn. (1) by a porosity-dependent thermal conductivity. Thermal conductivities are the geometric average between pore fluid (k_w) and matrix (k_m) conductivities (Deming & Chapman, 1989)

$$k = k_m^{1-\phi} k_w^\phi \quad (5)$$

The matrix conductivity is a material constant and the pore fluid conductivity is calculated according to Deming & Chapman (1989) for a constant temperature of $T = 100^\circ\text{C}$

$$k_w = a + bT + cT^2 \quad (6)$$

with $a = 0.565 \text{ Wm}^{-1}\text{K}^{-1}$, $b = 1.88 \times 10^{-3} \text{ Wm}^{-1}\text{K}^{-2}$, $c = -7.23 \times 10^{-6} \text{ Wm}^{-1}\text{K}^{-3}$ and T is temperature.

Airy isostatic equilibrium is ensured during each time step by a non-linear optimisation algorithm that computes the subsidence that minimises the weight difference between the lithospheric column before and after rifting, sedimentation, compaction and heat transfer.

The second implementation is the commercial basin modelling software TECMOD2D (<http://www.tecmod>).

com). TECMOD2D's forward model resolves simultaneously for basin-scale (e.g. sedimentation, compaction and maturation) and lithosphere-scale (e.g. rifting, flexure, heat transfer) processes. To fit a specific basin, TECMOD2D uses an inverse algorithm that automatically updates the crustal and mantle stretching factors as well as the water depth through time so that an input stratigraphy is fitted to a desired accuracy. The details of the automated basin reconstruction approach used in TECMOD2D are described in Rupke *et al.* (2008).

Reverse modelling

Probably the most classic and widely used technique for recovering the subsidence history from the stratigraphic record is the decompaction-backstripping analysis. The general concepts are described in Steckler & Watts (1978), Watts *et al.* (1982) and are summarised in the book by Allen & Allen (2005). For completeness, we will briefly review the approach here. The total subsidence history is computed by consecutively decompacting and compacting individual sediment packages. First the oldest sediment package is decompacted and moved up to a reference surface, i.e. the assumed palaeo-water depth, yielding the total subsidence at this time. Next the next younger sediment package is decompacted and moved up to the reference surface, whereas the older package(s) is compacted and moved downwards. This procedure is repeated for all sediment packages until the present day configuration is recovered and yields the total subsidence through time as well as the subsidence history for every sediment package.

A key assumption in this analysis is that the present sediment thicknesses are only affected by compaction and not by the stretching-induced thinning. As a consequence, total subsidence curves obtained from backstripping analysis may systematically underestimate sediment loading and subsidence, especially in basins that experienced multiple rift events.

FEEDBACKS BETWEEN SEDIMENTATION, STRETCHING AND HEAT FLOW

A key objective of basin modelling is to predict the basement heat flow history and thereby the thermal evolution of sedimentary basins and rifted margins. McKenzie (1978) showed for the instantaneous rifting case without sediments that heat flow peaks during the syn-rift phase and exponentially decays during post-rift equilibration. Higher stretching factors result in higher heat flows through time. But basement heat flow is not only controlled by stretching factors; it is also controlled by rift duration, sedimentation rate and thermal conductivity of the basin infill (Jarvis & McKenzie, 1980; Lucazeau & Ledouaran, 1985). The blanketing effect of sedimentation affects the heat flow in two ways: rapid sedimentation of cold material enhances the cooling of the crust (Debrenaecker,

1983; Wangen, 1995), but the usually lower thermal conductivities of the sediments can slow down post-rift cooling (Zhang, 1993). The net effect of thermal blanketing depends on the sedimentation rate (Tervoort & Bertotti, 1994) and the amount of stretching.

To investigate and evaluate the feedbacks between sedimentation, heat flow and stretching, we have performed a series of 1D forward model runs. These models assume a lithosphere thickness of 120 km and a crustal thickness of 40 km. The thermal conductivities (and diffusivities) of mantle ($3.3 \text{ W m}^{-1} \text{ K}^{-1}$), crust ($2.8 \text{ W m}^{-1} \text{ K}^{-1}$) and the sediment grains ($2 \text{ W m}^{-1} \text{ K}^{-1}$) are initially constant and radioactive heat production is not included. The surface porosity of the basin infill is 0.63, the compaction length c is 0.51 km^{-1} and the grain density is 2700 kg m^{-3} . The temperature at the top is fixed at 5°C ; the thermal boundary conditions at the base of the lithosphere are discussed in the following section.

Steady-state heat flow

For the steady-state case, the basement heat flow depends on the conductivities of the sediments and boundary conditions at the base of the lithosphere. Most commonly used is the plate model, which assumes constant temperatures at the base of the lithosphere (Jarvis & McKenzie, 1980). However, Doin & Fleitout (1996) and Prijac *et al.* (2000) suggest the alternative Chablis model (Constant Heat flow Applied to the Bottom Lithospheric Isotherm) to achieve better fits in long-term subsidence for some sedimentary basins. Figure 1 shows computed steady-state geotherms for various sediment conductivities and bottom-temperature boundary conditions. The left panel plot shows the results for the plate model and the right panel plot for the Chablis model. Regardless of boundary conditions, in the steady-state case the heat flow, $\vec{q} = -k \frac{\partial T}{\partial z}$, needs to be constant with depth. Consequently, at the sediment-crust interface, the basement heat flow needs to equal the heat flow in the sediments.

For the plate model, this implies that a change in sediment conductivity will also affect the thermal gradient in the crust and consequently basement heat flow as well. This is illustrated in the left panel plot of Fig. 1. The lower the sediment conductivity, the higher the thermal gradient in the sediments, and the lower the basement heat flow. This depression in basement heat flow is one effect of sediment blanketing and results directly from the fixed temperature boundary conditions at the top and bottom of the lithosphere.

In the Chablis model, the heat flow at the base of the lithosphere is constant and consequently, for the steady-state case, also the basement heat flow. The right panel plot of Fig. 1 shows that in the Chablis model also, sediment geothermal gradients increase with decreasing conductivity. However, as the basement heat flow is fixed, these higher geothermal gradients in the sediments do not decrease basement heat flow but shift crustal and mantle temperatures to higher values. The implications are that in the

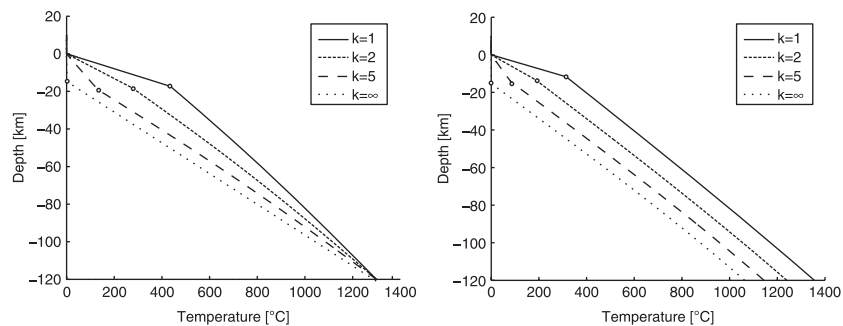


Fig. 1. Lithosphere geotherms for two different temperature boundary conditions at the base of the lithosphere. The left panel plot shows the results for a constant temperature and the right panel plot for a constant heat flow boundary condition (30 mW m^{-2}). Circles mark the sediment–basement interface. The different curves correspond to differing grain thermal conductivities. For both boundary conditions, sediment temperatures increase with decreasing thermal conductivity. In the case of a constant temperature boundary condition, basement heat flow is depressed by sedimentation; for a constant heat flow boundary condition, basement heat flow is constant but mantle temperatures increase with decreasing sediment conductivity. See text for details.

Chablis model sedimentation does not depress basement heat flow but results in higher temperatures at the lithosphere–asthenosphere boundary.

In summary, for both studied bottom boundary conditions lower sediment conductivities result in higher basin temperatures. In the plate model, which is commonly used in lithosphere-scale models, basement heat flow is depressed by sedimentation and the temperature at the base of the lithosphere is constant. In the Chablis model, implicitly used in basin-scale models where the basement heat flow is fixed, sedimentation does not affect basement heat flow but mantle temperatures increase with decreasing sediment conductivities. For the remainder of the paper, we will use the, in our view more appropriate, plate model and will next explore the temporal evolution of basement heat flow.

Time-dependent heat flow

Figure 2a illustrates the effects of sedimentation on basement heat flow through time. Three different example runs are shown in which the stretching factor is three and rifting occurs between 100 and 80 Ma. The thin solid line shows the predicted heat flow curve from the analytical McKenzie model for instantaneous rifting (McKenzie, 1978). The dashed line represents a model run for the finite rifting case but no sediments are deposited, and the thick solid line shows basement heat flow through time for a model where the basin is always completely filled with sediments. The analytical solution for instantaneous rifting shows, of course, the highest heat flow values through time. The dashed line shows the typical evolution; increasing values during the syn-rift phase and exponential decay during post-rift cooling. In the model that accounts for sedimentation, the heat flow curve is overprinted by the blanketing effect. The rapid deposition of cold sediments with low conductivity depresses heat flow during the syn-rift phase. The peak heat flow is $\sim 40\%$ lower than the peak heat flow predicted by the analytical solution. Note that, consistent with the previous section, sedimentation

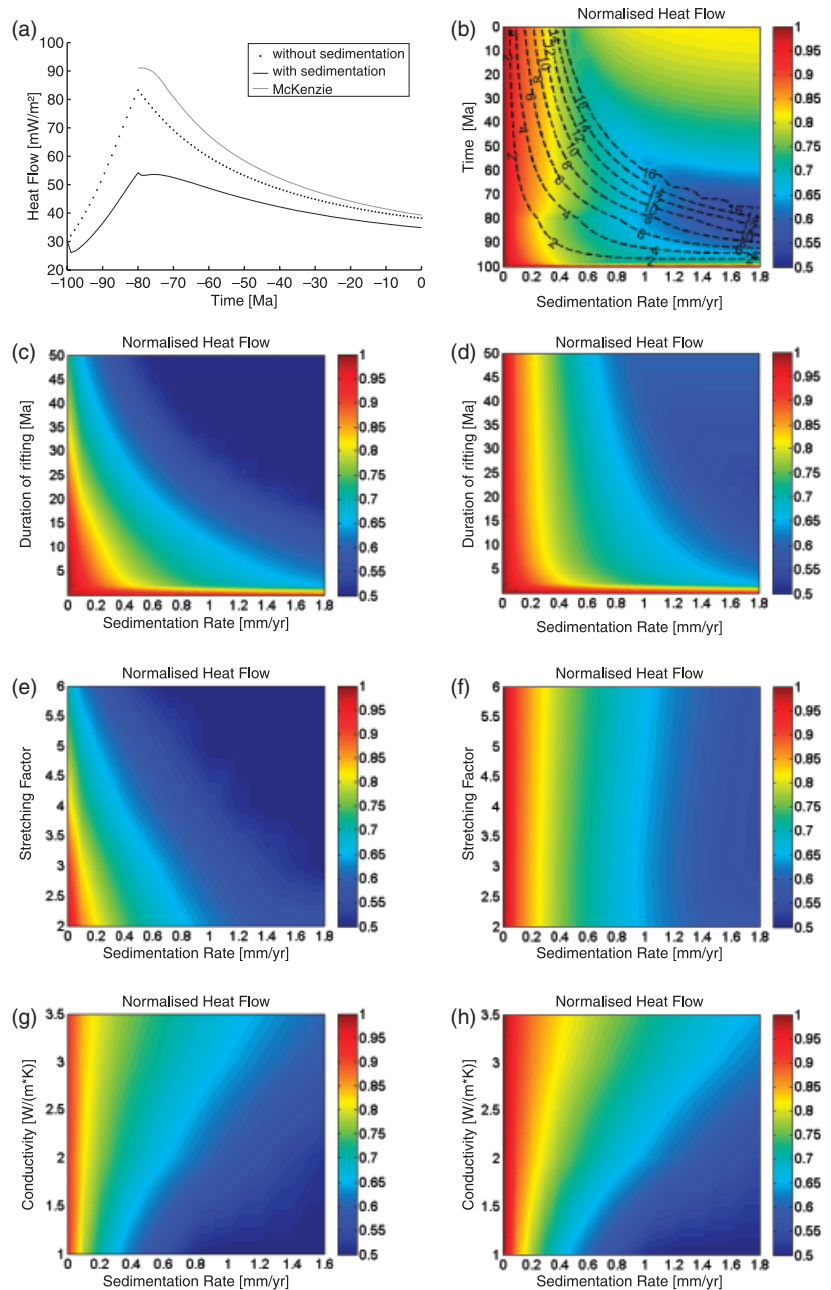
also changes the stable steady-state geotherm, which is apparent from the long-term depression in heat flow during the post-rift phase.

Figure 2b shows that the predicted depression in (post-rift) basement heat flow increases with higher sedimentation rates. In Fig. 2b, the results for a series of model runs with the same parameters used in Fig. 2a but with varying sedimentation rates are shown. Basement heat flow is normalised to a model without sedimentation (dotted line in Fig. 2a). For low sedimentation rates ($< 0.2 \text{ mm year}^{-1}$), the results are similar and the normalised heat flow is above 0.9. For intermediate rates ($0.2\text{--}0.5 \text{ mm year}^{-1}$), both the steady-state and peak syn-rift heat flow are depressed by 25–35%. For high rates ($> 0.5 \text{ mm year}^{-1}$), the peak heat flow is about 40–50% lower, whereas the steady-state heat flow is less affected. This results from the rapid sedimentation during the syn-rift and early post-rift phase, so that the basin is completely filled at late post-rift times. In this case, the system can equilibrate and steady-state conditions are reached.

Parameter study

The efficiency of 1D basin models allows for detailed sensitivity tests of these results to variations in model parameters including rift duration, stretching factor and sediment conductivity. Figure 2c and d show contour plots of peak heat flow at the end of the syn-rift phase as a function of rift duration and sedimentation rate. The stretching factor is constant ($\beta = 3$). In (c) the heat flow is normalised to the analytical McKenzie solution and in (d) to a forward model without sedimentation. It is clear from (c) that the McKenzie model is only valid if stretching is quasi-instantaneous and occurs for $< 20\text{--}25 \text{ Ma}$ and if sedimentation rates are low ($< 0.2 \text{ mm year}^{-1}$). Higher duration of stretching leads to lower heat flow values (25–40%) even for low sedimentation rates. Figure 2d shows that excluding the sediments from the temperature solution may lead to a significant overestimation of the basement heat flow even if finite rift durations are

Fig. 2. (a) Comparison of heat flow development through time for different scenarios. The black line corresponds to a model with sedimentation; the dashed line shows the heat flow evolution of a model assuming water infill and the grey line is calculated with the analytical McKenzie solution. The thick sedimentary sequence suppresses the syn-rift heat flow and the maximum heat flow at the end of rifting. During the post-rift time, the decrease in heat flow is slower than for the model without sediments. (b) Phase diagram showing the normalised heat flow evolution for different sedimentation rates. Rifting occurs between 100 and 80 Ma, the heat flow is normalised to a model without sedimentation. The dashed lines outline the sediment thickness. (c) and (d) show normalised peak syn-rift heat flow as a function of rift duration and sedimentation rate for constant stretching ($\beta = 3$). The heat flow is normalised against the analytical solution for instantaneous stretching (c) and the results assuming no sedimentation but different rift durations (d). Plots (e) and (f) show the results for stretching between 100 and 80 Ma with varying thinning factors and sedimentation rates. In (g) and (h) the influence of grain thermal conductivity of the sediments is shown. Contours show normalised peak syn-rift heat flow; the left panel plot is normalised to the analytical solution and the right panel plot to a model without sediments.



accounted for. For long rift durations and high sedimentation rates, the basement heat flow is $\sim 50\%$ lower than in models that exclude the sediments from the thermal solution.

In a second series of model runs, we have explored the effect of variations in stretching factors and sedimentation rates. Rifting occurs between 100 and 80 Ma. Figure 2e and f show contour plots of the peak syn-rift basement heat flow as a function of stretching factor and sedimentation rate. Again (e) is normalised to the analytical solution and (f) is normalised to a model without sedimentation. Figure 2e shows that the McKenzie solution is again only valid for very low sedimentation rates in combination with low stretching factors. Even if the finite rift duration is taken

into account (f), basement heat flow can be depressed by $\sim 50\%$ for high sedimentation rates.

The effects of variations in sediment thermal conductivity are two-fold: firstly, the lower the conductivity of the infill, the higher are the temperatures in the basins and the lower is the basement heat flow (Figs 1, 2g and h). Secondly, low thermal conductivities slow down post-rift cooling. The effects of sedimentation on basement heat flow therefore increases with lower sediment conductivities. This is illustrated in Fig. 2g and h, where peak syn-rift heat flow is plotted vs. sedimentation rate and infill conductivity. The heat flow in (g) is normalised to the analytical solution and in (h) to a model without sediments. These plots show that for realistic grain conductivities ($< 3 \text{ W m}^{-1} \text{ K}^{-1}$) and

sedimentation rates ($>0.3 \text{ mm year}^{-1}$), basement heat flow is greatly reduced with respect to the reference solutions to which the plots are normalised.

Implications and discussion

In summary, the synthetic models have clearly confirmed the blanketing effect of sedimentation. Rapid sedimentation of cold low conductivity sediments depresses the syn-rift and steady-state heat flow. The blanketing effect is highest for high sedimentation rates and low grain conductivities. The systematic parameters study has shown that even for moderate sedimentation rates ($\sim 0.2 \text{ mm year}^{-1}$), the sediments should be included in the thermal solution. Differences in basement heat flow between models that include sediments in the thermal solution and models that do not reach up to 50%. We therefore conclude that it is important to consider the thermal evolution in the sediments to obtain a realistic basement heat flow development through time. For realistic parameter choices, the basement heat flow evolution is complex and should not be treated as a boundary condition.

CASE STUDY – VØRING BASIN

In order to test how important the various feedbacks between basin and lithosphere-scale processes are in real world case studies, we have performed a series of reconstructions of the Vøring Basin in the Norwegian Sea. The Vøring Basin is part of the Norwegian Volcanic Margin and is well-suited for the objectives of this study. Extensive hydrocarbon exploration has generated lots of data for model testing and numerous previous modelling studies can be used to benchmark and cross check our findings (Talwani & Eldholm, 1972; Skogseid & Eldholm, 1989; Mjelde *et al.*, 2003; Wangen *et al.*, 2008). We will apply the automated basin reconstruction approach described in 'Basin-modelling approaches' to reconstruct the Vøring continental margin with special emphasis to the sedimentation rates, evolution of the palaeo water depth and palaeo-heat flow and the feedbacks between these processes.

Geological Setting of the Vøring Basin

The Vøring sedimentary basin is located at the Norwegian continental shelf between 64 and 68°N and 2 and 10°E (Fig. 3). The Bivrost lineament and the Jan Mayen lineament separate the Vøring Basin from the adjacent Ribban and Vestfjord Basin to the north and the More Basin to the south, respectively. The basin is part of the mid-Norwegian margin which developed through several rift episodes since the end of the Caledonian orogeny (Talwani & Eldholm, 1972). The lithospheric separation was preceded and accompanied by uplift and flood basalt volcanism that constructed the Vøring marginal high (Ren *et al.*, 2003).

The number and timing of rift episodes are still debated but there is an agreement considering a major rift event during the late Jurassic (Doré *et al.*, 1999; Brekke, 2000;

Skogseid *et al.*, 2000) and the onset of seafloor spreading and break-up taking place about 55–54 Ma (Gernigon *et al.*, 2006; Faleide *et al.*, 2008; Wangen *et al.*, 2008). The main difference between the proposed rift phases is a mid-Cretaceous rifting. Fjeldskaar *et al.* (2008) describe seismic and stratigraphic evidence in the Vøring Basin and modelled an extension event at 95 Ma, whereas Skogseid *et al.* (2000) and Færseth & Lien (2002) argued that there is no evidence for mid-Cretaceous extension in the Vøring Basin. The discussed rift intervals are summarised in Wangen *et al.* (2008).

The Euromargin transect 2 across the Vøring Basin is 320 km long (Fig. 4) and can be subdivided into structural highs and sub-basins. The northwestern part comprises of three about 15-km-deep depocentres (from NW to SE): Hel Graben, Någrind Syncline and Træna Basin separated by the Nyk High and Utgard High. The southeastern part is generally shallower; the Helgeland Basin is about 8 km deep.

Reference model

Model set up

We created a reference model for the reconstruction of the Vøring Basin with an initial crustal thickness of 35 km and an isostatic compensation depth of 120 km. The input stratigraphy for the modelled transect is shown in Fig. 4. The temperature at the asthenosphere lithosphere boundary is 1300 and 5 °C at the seafloor and atmosphere; radiogenic heat production in the continental crust decreases exponentially with a depth from a maximum value of $2 \mu\text{Wm}^{-3}$; radiogenic heating in the sediments is set to $1 \mu\text{Wm}^{-3}$. The material properties representing each stratigraphic unit and the crust and mantle are summarised in Tables 1 and 2, respectively. We assume three rift phases for the reference model:

- (1) 290–146 Ma to account for the Late Palaeozoic–early Mesozoic rifting with the main rift phase during the Jurassic,
- (2) A short mid-Cretaceous rifting 100–94 Ma and
- (3) Rifting during upper Cretaceous until break-up at the Palaeocene–Eocene transition 80–56 Ma.

The effective elastic thickness is 5 km and the necking level 15 km (Reemst & Cloetingh, 2000; Fjeldskaar *et al.*, 2004; Rüpke *et al.*, 2008).

Stratigraphy and well comparison

A comparison between the input and modelled stratigraphy for the reference model is shown in Fig. 5. The residual error after 20 iterations is around 5%. In addition, to the stratigraphy comparison, basin temperature and maturity of the reconstruction has been compared with borehole data to further verify the modelling results. An indicator of thermal maturity is vitrinite reflectance, $R_o\%$, (Sweeney & Burnham, 1990), which is sensitive to time and tem-

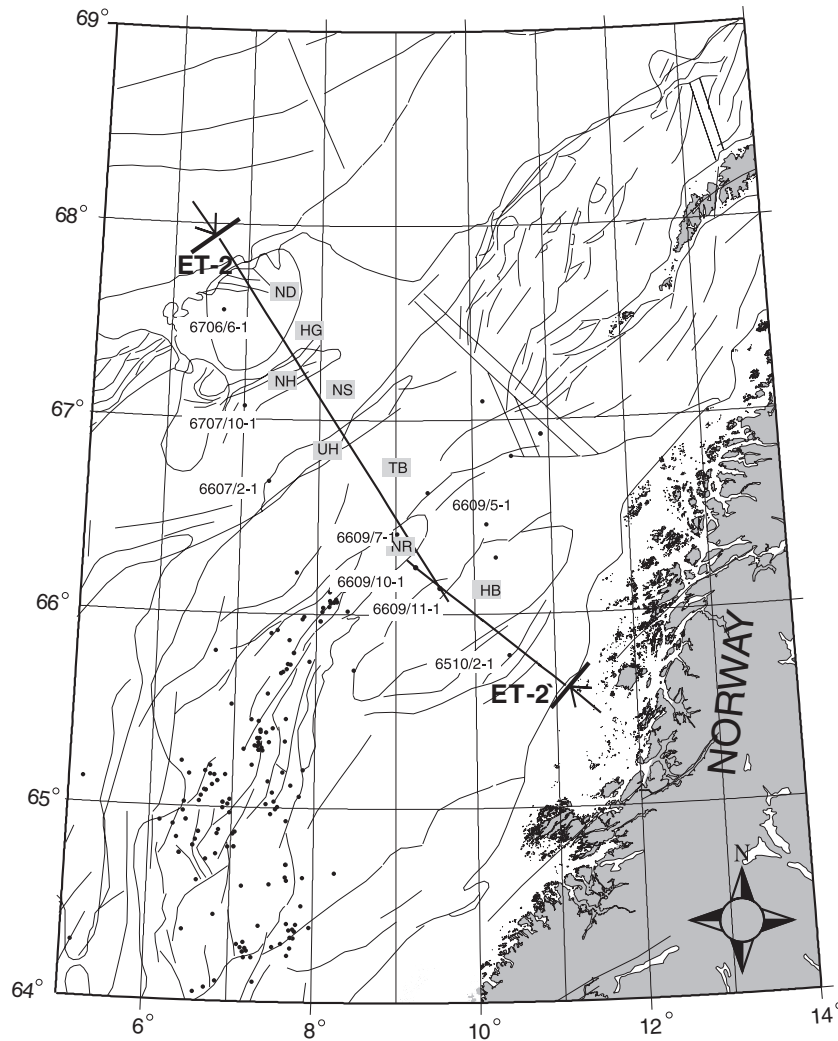


Fig. 3. Location of the modelled EUROMARGIN transect 2 and main structural features on the Vøring margin. The location of wells is shown by the black dots. The data used in this study are derived from the labelled wells. ND, Naglfar Dome; HG, Hel Graben; NH, Nyk High; NS, Någrind Syncline; UH, Utgard High; TB, Træna Basin; NR, Nordland Ridge; HB, Helgeland Basin, modified from Faleide *et al.* (2008).

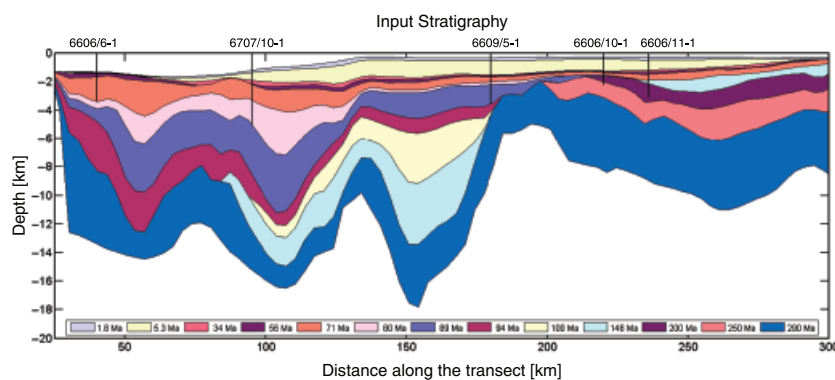


Fig. 4. The input stratigraphy used for the modelling is shown in the top. The wells are projected onto the transect. TCB, Top Crystalline Basement; BC, Base Cretaceous; TA, Top Albian; TC, Top Cenomanian; TT, Top Turonian; IC, Intra Campanian; BM, Base Maastrichtian; TP, Top Palaeocene; TE, Top Eocene; BP, Base Pliocene; BPI, Base Pleistocene; SF, Seafloor.

perature and can therefore be used to check the thermal solution.

Seven wells are located near the transect; for four wells, both vitrinite reflectance and temperature data are avail-

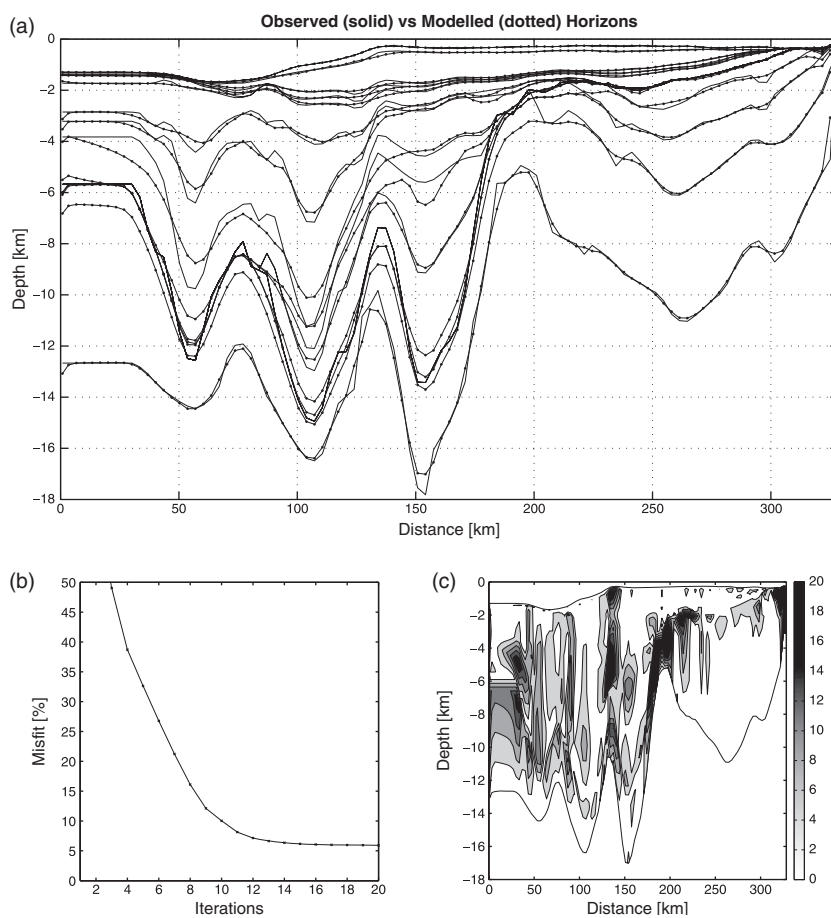
able, for one well only temperature and for two wells only vitrinite reflectance data exist. Figure 6 shows a comparison of the modelled and observed data for three wells. Well 6710/10-1 is located at 95 km, well 6609/10-1 at 220 km and

Table 1. Rock properties of the stratigraphic layers (Fig. 4)

Formation	Age (Ma)	Density (kg m^{-3})	Thermal expansion (K^{-1})	Vol. heat (Wm^{-3})	Heat capacity ($\text{Jkg}^{-1}\text{K}^{-1}$)	Grain conductivity ($\text{Wm}^{-1}\text{K}^{-1}$)	Surface porosity (%/100)	Compaction length (km^{-1})
Silty shale Triassic	208–290	2680	0	10^{-6}	1000	2.1	0.5	0.32
Silty shale Jurassic	145–208	2720	0	10^{-6}	1000	2.1	0.6	0.46
Silty shale Early Cretaceous	95–145	2720	0	10^{-6}	1000	2.1	0.6	0.46
Silty shale Late Cretaceous	65–95	2700	0	10^{-6}	1000	2.1	0.6	0.35
Shale Palaeocene	50–65	2700	0	10^{-6}	1000	2.1	0.6	0.41
Silty shale Eocene	34–50	2700	0	10^{-6}	1000	2.1	0.6	0.51
Silty shale Oligocene	3–34	2700	0	10^{-6}	1000	2.1	0.63	0.51
Sand Pliocene	0–3	2700	0	10^{-6}	1000	1.7	0.63	0.51

Table 2. Material properties of the crust and mantle

	Density (kg m^{-3})	Thermal expansion (K^{-1})	Vol. heat (Wm^{-3})	Thermal conductivity ($\text{Wm}^{-1}\text{K}^{-1}$)
Upper crust	2700	2.4×10^{-5}	2×10^{-6}	3
Lower crust	2900	2.4×10^{-5}	2×10^{-6}	3
Lithospheric Mantle	3340	3.2×10^{-5}	0	3.5

**Fig. 5.** Results of the modelling (a) The observed input stratigraphy (solid lines) is compared with the modelled stratigraphy (dotted lines), (b) Residual misfit for every iteration step, (c) The distribution of the residual error is shown. The average residual error after 20 iterations is $< 5\%$.

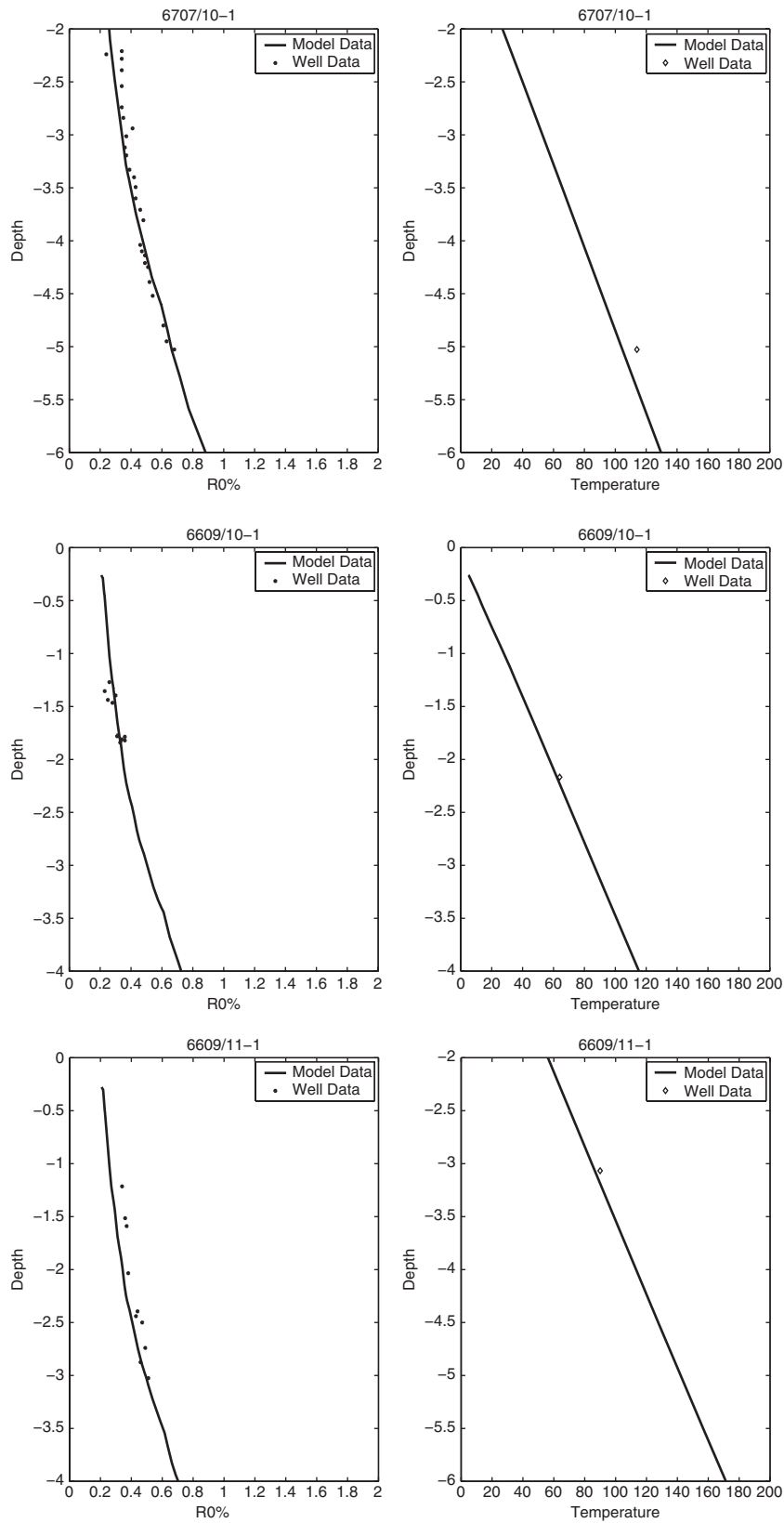


Fig. 6. Comparison of modelled and observed data for different wells. On the left side, the computed vitrinite reflectance (solid line) is compared with the modelled data (dots). The temperature comparison is shown in the right side. The modelled data are displayed as solid lines and the well data as diamonds. Both the temperature and vitrinite reflectance data fit very well the well data.

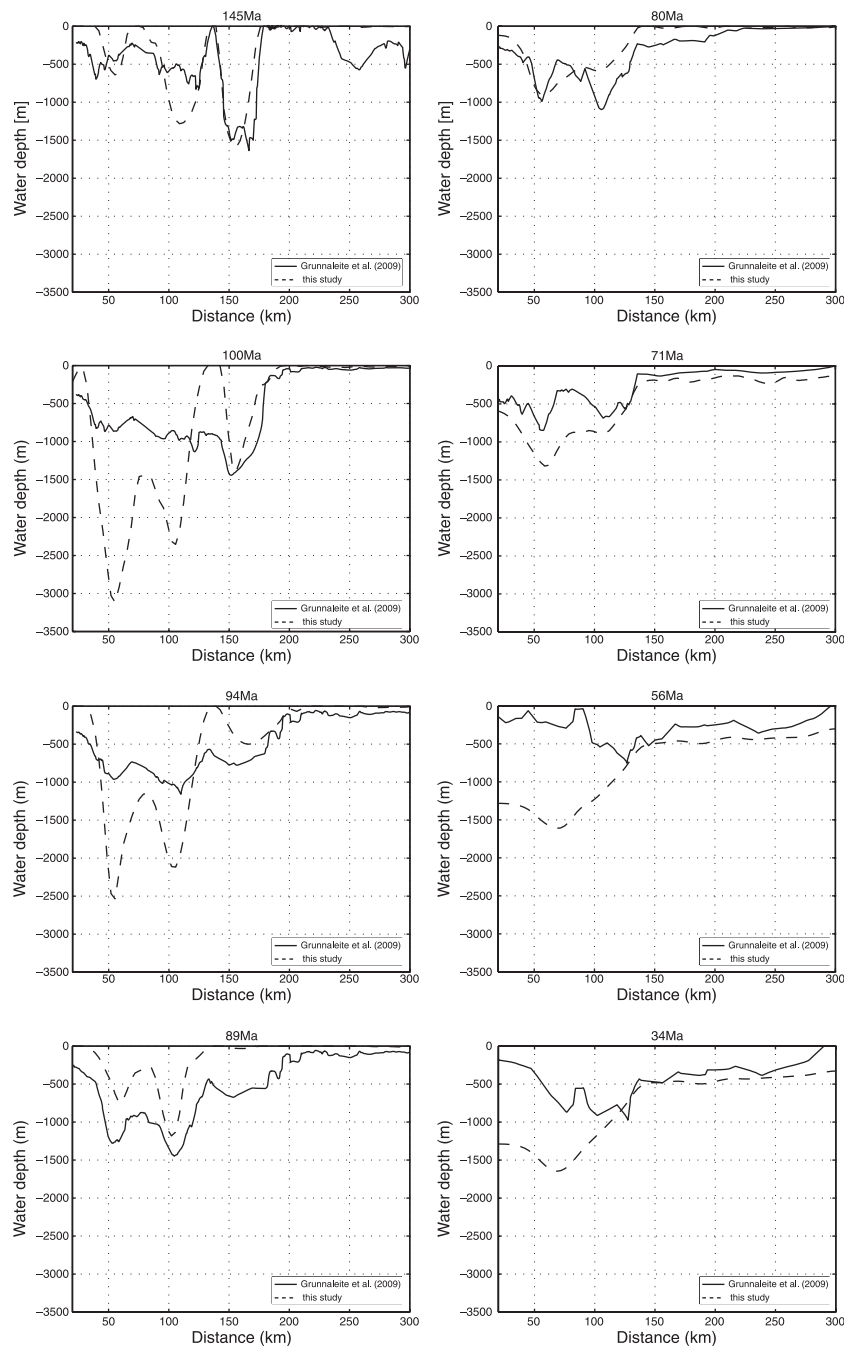


Fig. 7. Palaeo-water depth at different time steps. The solid lines represent the data from Grunnaleite *et al.* (2009), the dashed line is the computed water depth. Discrepancies are due to the uncertainties of the input stratigraphy (100 and 94 Ma) and break-up related features (56–5 Ma).

well 6609/11-1 at 236 km along the profile. At all wells, the computed temperatures match the present-day temperatures. The vitrinite data are fitted very well too, which indicates that cumulative heat flow through time is modelled correctly.

Palaeo-water depth

Reconstructions of water depth derived from structural consideration and microfossils for wells near the modelled

transect for the Quaternary to Cretaceous are available from Grunnaleite *et al.* (2009). Figure 7 shows palaeo-water depth predicted by TECMOD2D's automated basin fitting algorithm together with the data by Grunnaleite *et al.* (2009). The general trends in palaeo-water depth are reproduced by the reference model, although the absolute values do show some deviations. The differences during the mid-Cretaceous (100 and 94 Ma) are a result of the input stratigraphy. In the eastern part, the Cretaceous layers are very thin or missing, and for both the Top Albian and the

Top Cenomanian horizons in the western part, data are only available for about 80 km along the transect. As a consequence, no or only limited sedimentation occurs in the model at these times where horizons are thin or missing and water depth increases due to syn-rift and post-rift subsidence. The interpretation of the base Cretaceous and the layers underneath are also uncertain (Wangen *et al.*, 2008). Differences are also observed at the end of rifting and after break-up. In our models, no changes in water depth are observed after break-up whereas the data of Grunnaleite *et al.* (2009) show increasing water depths after break-up. The post-break-up subsidence implies a higher heat input into the system than modelled in our reconstruction, which could be a break-up related feature or a result of magmatic underplating, both of which are not included in our models. An alternative explanation for rapid post-break-up subsidence could be mineral phase transitions as suggested by Simon & Podladchikov (2008) and Kaus *et al.* (2005). Except for the discrepancies during the mid-Cretaceous and after break-up, the trends in sea-level change are fitted well.

Thinning factors

Thinning is highest at the three depocentres, the cumulative stretching factor (β) after three periods of rifting is 4.9 at Hel Graben, 4.8 at N agrind Syncline and 3.8 at the Tr ena Basin (Fig. 8). Figure 8 shows that the eastern part of the basin is mainly formed during the first rift event, whereas the second and third rift phases formed the western part. These observed westward migration of stretching is in accordance with the studies of Reemst & Cloetingh (2000), Gernigon *et al.* (2006) and Wangen *et al.* (2008).

The three observed maxima in total crustal thinning beneath the Tr ena Basin, N agrind Syncline and Hel Graben are in good agreement with the stretching described by Reemst & Cloetingh (2000), ($\beta = 3.9$ for Tr ena Basin, $\beta = 5.3$ for N agrind Syncline and $\beta = 4.1$ for Hel Graben) and Wangen & Faleide (2008). Somewhat higher values

are reported by Wangen *et al.* (2008) who calculated stretching factors of 8, 6 and 3.5 for Tr ena Basin, N agrind Syncline and Hel Graben, respectively

Sedimentation and heat flow

The distributions of the sedimentation rates along the transect are shown in Fig. 9a. The highest sedimentation rates can be observed during and after the second rift phase, during the upper Cretaceous, at all depocentres, which is similar to the findings of Wangen *et al.* (2008) and F arseth & Lien (2002). Wangen *et al.* (2008) described rates of several hundred metres per million years during the mid-Cretaceous to Palaeocene. The Tr ena Basin and the N agrind Syncline show high post-rift sedimentation after the first rift episode, whereas nearly no sedimentation occurred at the westernmost Hel Graben. Sedimentation rates frequently exceed 0.5 mm year^{-1} and reach peak values of 1.5 mm year^{-1} , which indicates that blanketing effects should be important during the formation of the V oring Basin.

Figure 9b shows the heat flow evolution plotted with time for the V oring Basin. The computed variations in present day (0 Ma) heat flow values coincide with the stratigraphy; relatively high values are observed at the Highs (e.g. Nyk High at 80 km and Utgard High at 130 km) and comparably lower values occur at the depocentres [e.g. Hel Graben (57 km), N agrind Syncline (105 km) and Tr ena Basin (153 km)]. The long-term decrease results both from sediment deposition (cf. 'Feedbacks between sedimentation, stretching and heat flow') and from reduced radiogenic heating due to crustal thinning. The effect of blanketing becomes obvious at the end of the first rift phase. The heat flow decreases rapidly during times of high sedimentation rates (dashed white circle) at N agrind Syncline, whereas in comparison only a moderate decrease in heat flow is seen at Hel Graben. This decrease coincides with the low sedimentation rates observed at that time (white circle).

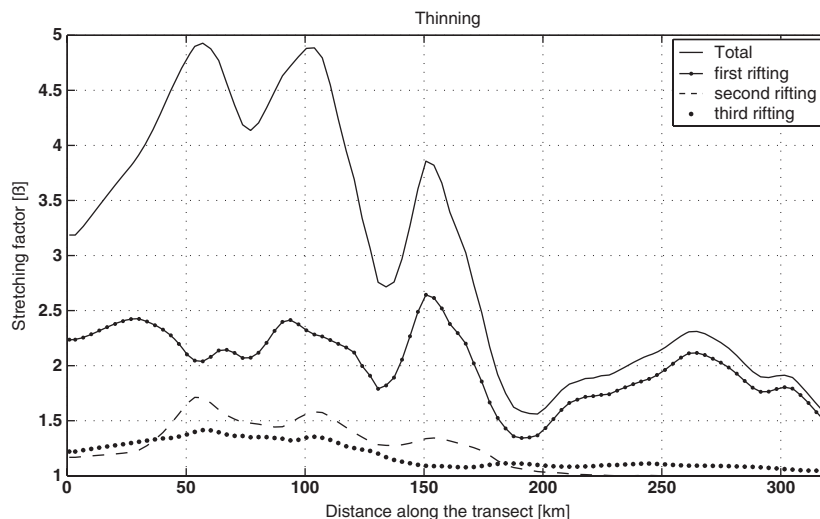


Fig. 8. Total stretching factor and stretching for each rift phase is plotted against the distance along the profile.

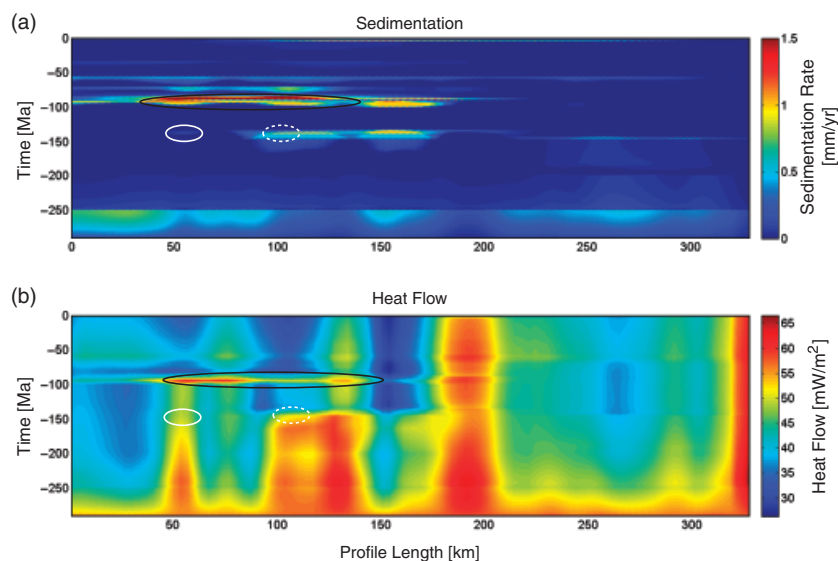


Fig. 9. (a) Variations of sedimentation is plotted with modelling time and distance along the transect. High sedimentation is observed during the Cretaceous for the three depocentre, Hel Graben, Nâgrind Syncline and Træna Basin. (b) A decrease in heat flow coincides with increasing sedimentation rates. See text for details.

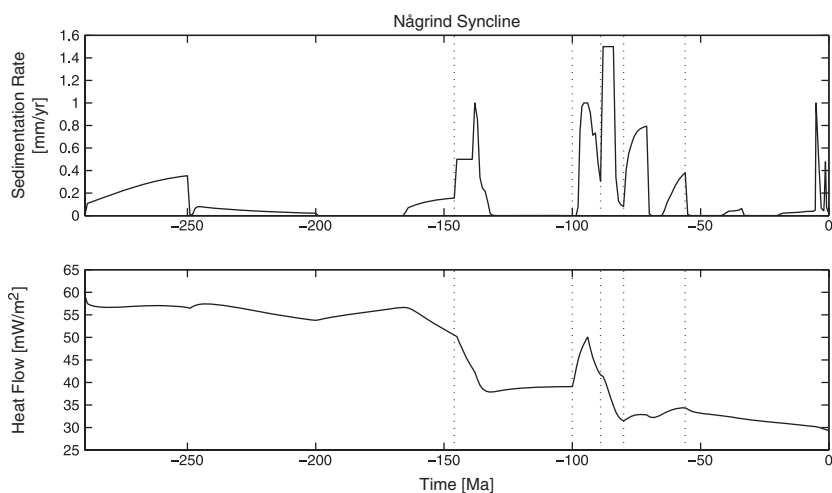


Fig. 10. Sedimentation Rate and Heat Flow at Nâgrind Syncline (105 km). The heat flow is depressed during times of high sedimentation.

At the beginning of the second rift phase (100 Ma), the heat flow increases from Hel Graben to Træna Basin (black circle). As soon as the sedimentation rates reach high values (black circle in Fig. 9a), heat flow decreases by 15–20 mW m⁻², which is most clearly observed at the depocentres.

Figure 10 illustrates the feedbacks between sedimentation, and basement heat flow for the Nâgrind Syncline at 105 km in detail. The heat flow increases during extension but at the onset of sedimentation, the heat flow decays very rapidly. At the beginning of rifting (beginning of modelling time), the basement heat directly decreases due to the high sedimentation rates. In total, the calculated basement heat flow decreases from about 60 mW m⁻² at beginning of rifting to about 30 mW m⁻² at the present time for the Nâgrind Syncline. Our values are lower compared with ~40–50 mW m⁻² described in Wangen *et al.* (2008) but

they did not include stretching in the sedimentary part of the basin.

Sensitivity to model parameters

The good fit of the input stratigraphy and the cross-check of the reconstruction against independent temperature, vitrinite and palaeobathymetry data suggest that the reference model is a valid approximation of the structural and thermal evolution of the modelled transect. To test the sensitivity of the reference model to variations in model parameters, we have run a series of reconstructions with e.g. differing initial crustal thickness, uniform and differential thinning scenarios, and variations in rift phases. In particular, we have explored the effects of differences in time and duration of the mid-Cretaceous rift phase (cf. 'Geological Setting of the Vøring Basin'). The basin

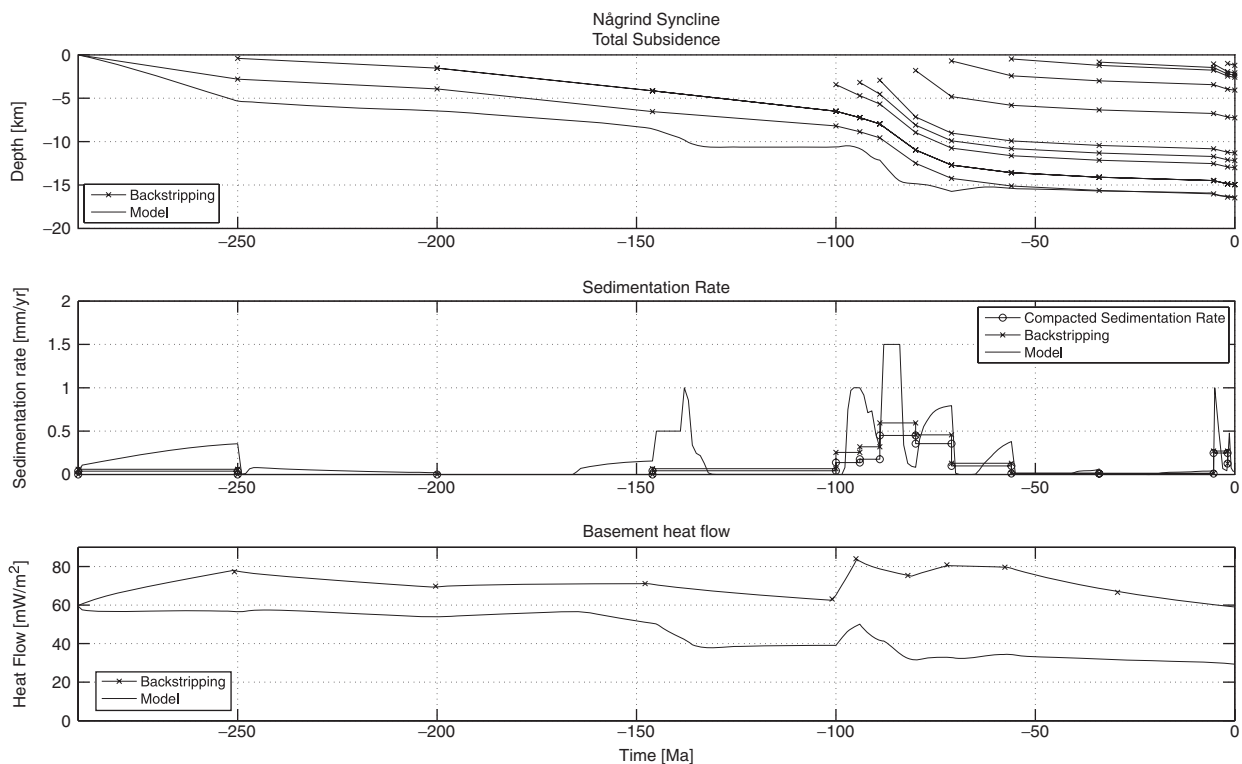


Fig. 11. Comparison of the results obtained from decompaction/backstripping analysis and lithosphere-scale forward modelling. The top panel plot shows basement subsidence from the forward modelling (solid line) and total subsidence of every sedimentary layer from the backstripping analysis (crosses). The difference in total basement subsidence is equal to the crustal stretching factor calculated at that time step and results from the fact that sediments are stretched/thinned with the crustal stretching factor in the forward model. The middle plot shows predicted sedimentation rates computed with three different methods. Sedimentation rates are highest in the forward model, which results again from thinning of the sediments. Decompacted and compacted sedimentation rates are consistently lower. The lower panel plot shows the predicted basement heat flow for the forward model (solid line) and for a model based on tectonic subsidence obtained from backstripping analysis without sediments (crosses). The backstripping methods lead to higher basement heat flow values compared with the results from the forward modelling. The effects of thermal blanketing can be seen when sedimentation rates are highest (e.g. 146 and 94 Ma).

stratigraphy and well data can be fitted also with the different model configurations but we achieved the best fit with parameters assumed in the reference model. Especially water depth can be matched most closely with the reference model parameters.

One additional model has been performed excluding radioactive heat generation to verify the observed feedbacks between sedimentation and basement heat flow from the synthetic models in a more complex set up. This model confirms the influence of sedimentation discussed in 'Feedbacks between sedimentation, stretching and heat flow' and 'Reference Model'. Heat is depressed during times of high sedimentation and the long-term decrease is caused by both sedimentation and crustal thinning resulting in reduced radiogenic heat generation.

Comparison with backstripping analysis

Figure 11 shows the differences in total subsidence, sedimentation rates and basement heat flow for both modelling approaches, the classic backstripping method and the forward modelling-based TECMOD2D reconstruc-

tion. The black crosses show the location of every layer at every time step calculated with backstripping. The solid line shows the subsidence history of the basin through time for the reference model. The total subsidence at the end of the modelling time is the same but there are differences in the evolution of subsidence. The subsidence calculated with TECMOD2D differs from the backstripping subsidence by the stretching factor calculated at that time step, which demonstrates that this difference is due to the stretching of the sedimentary infill. The subsidence calculated only through decompaction/backstripping without stretching the sediments and considering the thermal development of the sediments during stretching underestimates the subsidence and therefore, also the sedimentation rates. This is illustrated in the middle panel plot of Fig. 11, where sedimentation rates computed with three different methods are plotted. The highest rates occur in the reference model which is due to the stretching of the sediments and the higher temporal resolution (~ 1 Ma time stepping). Decompaction/backstripping-based sedimentation rates are consistently lower than in the reference model, which results from averaging over the total

time span of the sediment package considered and neglecting the effect of sediment thinning at times of crustal stretching. Compacted sedimentation rates are, of course, even lower and are shown for reference.

These differences in sedimentation rates again influence the heat flow due to the effects of blanketing described above. Figure 11 (bottom) shows the example of the Nāgrind Syncline at 105 km. The figure compares the basement heat flow between the reference model (same as in Fig. 10) and a separate 1D forward model with identical parameters except that sedimentation is neglected. This forward model without sedimentation is equivalent to an extended McKenzie type model that matches the tectonic subsidence curve obtained from the backstripping analysis. The predicted heat flow from this type of model is frequently used as a boundary condition in basin scale models. The offset between both heat flow curves, therefore, illustrates the differences between fully coupled lithosphere-scale models and backstripping-based basin-scale models. The basement heat flow is generally lower for the model including sedimentation and episodes of high sedimentation are clearly distinguishable by decreasing heat flow (e.g. 94 and 146 Ma). Differences in predicted heat flow reach up to 50%, which shows that blanketing effects are important during the evolution of the Vøring Basin and that backstripping-based approaches may underestimate both total subsidence as well as basement heat flow.

CONCLUSIONS

We have studied the feedbacks between basin and lithosphere processes with forward basin models to evaluate the blanketing effect of sedimentation on crustal heat flow in synthetic models. To study the implications in a case study, the Vøring Basin has been reconstructed using the classic backstripping analyses and the coupled forward model. The forward model fits well the present-day stratigraphy, temperature and vitrinite data as well as palaeo-water depth. Variations compared with results from the backstripping method can be explained and confirm the results of the synthetic models.

The key findings of this study are:

- The blanketing effect of sedimentation on crustal heat flow has been studied with simple synthetic models and it is largest for high sedimentation rates and sediments with low thermal conductivities.
- Differences in predicted heat flow between models that include the sediments in the thermal solution and models that do not, can reach up to 50%. This shows that basin models must resolve for all the feedbacks between lithosphere and basin-scale processes.
- We find considerable differences between the classic backstripping method and the forward modelling technique in sedimentation rates and subsidence curves (total and tectonic subsidence). The decompac-

tion method underestimates sedimentation rates, because the sedimentary part of the basin is not thinned.

- Reconstructed heat flow curves for the Vøring Basin show differences of up to 50% between models that include and do not include sedimentation.

ACKNOWLEDGEMENTS

The authors thank Stefan Schmalholz and one anonymous referee for their helpful formal reviews and Dani Schmid for his constructive informal review of this paper. Thanks also to GeoModelling Solutions for access to their basin-modelling tools.

REFERENCES

- ALLEN, P.A. & ALLEN, J.R. (2005) *Basin Analysis: Principles and Applications*, 2nd edn. Blackwell Publishing, Oxford.
- ATHY, L.F. (1930) Density, porosity, and compaction of sedimentary rocks. *AAPG Bull.*, **14**, 1–24.
- BREKKE, H. (2000) The tectonic evolution of the Norwegian Sea continental margin with emphasis on the Vøring and More Basins. In: *Dynamics of the Norwegian Margin* (Ed. by A. Nottvedt, S. Olaussen, B. Torudbakken, R.H. Gabrielsen, H. Brekke, O. Birkeland & J. Skogseid), *Geol. Soc. Spec. Publ.*, **167**, 327–378.
- DEBREMAECKER, J.C. (1983) Temperature, subsidence, and hydrocarbon maturation in extensional basins – a finite-element model. *AAPG Bull.-Am. Assoc. Petrol. Geol.*, **67**, 1410–1414.
- DEMING, D. & CHAPMAN, D.S. (1989) Thermal histories and hydrocarbon generation – example from Utah–Wyoming Thrust Belt. *AAPG Bull.-Am. Assoc. Petrol. Geol.*, **73**, 1455–1471.
- DOIN, M.P. & FLEITOUT, L. (1996) Thermal evolution of the oceanic lithosphere: an alternative view. *Earth Planet. Sci. Lett.*, **142**, 121–136.
- DORÉ, A.G., LUNDIN, E.R., JENSEN, L.N., BIRKELAND, O., ELIASSEN, P.E. & FICHLER, C. (1999) Principal tectonic events in the evolution of the northwest European Atlantic margin. In: *Petroleum Geology of Northwest Europe: Proceedings of the 5th Conference* (Ed. by A.J. Fleet & S.A.R. Boldy), pp. 41–61. Geological Society, London.
- FÆRSETH, R.B. & LIEN, T. (2002) Cretaceous evolution in the Norwegian Sea – a period characterized by tectonic quiescence. *Mar. Petrol. Geol.*, **19**, 1005–1027.
- FALEIDE, J.I., TSİKALAS, F., BREIVIK, A.J., MJELDE, R., RITZMANN, O., ENGEN, O., WILSON, J. & ELDHOLM, O. (2008) Structure and evolution of the continental margin off Norway and Barents Sea. *Episodes*, **31**, 82–91.
- FJELDSKAAR, W., HELSET, H.M., JOHANSEN, H., GRUNNALEITEN, I. & HORSTAD, I. (2008) Thermal modelling of magmatic intrusions in the Gjallar Ridge, Norwegian Sea: implications for Vitrinite reflectance and hydrocarbon maturation. *Basin Res.*, **20**, 143–159.
- FJELDSKAAR, W., TER VOORDE, M., JOHANSEN, H., CHRISTIANSON, P., FALEIDE, J.I. & CLOETINGH, S. (2004) Numerical simulation of Rifting in the Northern Viking Graben: the mutual effect of Modelling parameters. *Tectonophysics*, **382**, 189–212.
- GERNIGON, L., LUCAZEAU, F., BRIGAUD, F., RINGENBACH, J.C., PLANKE, S. & LE GALL, B. (2006) A moderate melting model

- for the Vøring Margin (Norway) based on structural observations and a Thermo-Kinematical Modelling: implication for the meaning of the lower Crustal bodies. *Tectonophysics*, **412**, 255–278.
- GRUNNALLEITE, I., FJELDSKAAR, W., WILSON, J., FALEIDE, J.I. & ZWIEGEL, J. (2009) Effect of local variations of vertical and horizontal stresses on the Cenozoic structuring of the Mid-Norwegian Shelf. *Tectonophysics*, **470**, 267–283.
- JARVIS, G.T. & MCKENZIE, D.P. (1980) Sedimentary basin formation with finite extension rates. *Earth Planet. Sci. Lett.*, **48**, 42–52.
- KAUS, B.J.P., CONNOLLY, J.A.D., PODLADCHIKOV, Y.Y. & SCHMALHOLZ, S.M. (2005) Effect of mineral phase transitions on Sedimentary Basin subsidence and uplift. *Earth Planet. Sci. Lett.*, **233**, 213–228.
- KOOI, H., CLOETINGH, S. & BURRUS, J. (1992) Lithospheric necking and regional isostasy at extensional basins .1. Subsidence and gravity modeling with an application to the Gulf of Lions Margin (Se France). *J. Geophys. Res.-Solid Earth*, **97**, 17553–17571.
- KUSZNIR, N.J. & ZIEGLER, P.A. (1992). The Mechanics of Continental Extension and Sedimentary Basin Formation – a Simple-Shear Pure-Shear Flexural Cantilever Model. *Tectonophysics*, **215**, 117–131.
- LUCAZEAU, F. & LEDOUARAN, S. (1985) The blanketing effect of sediments in basins formed by extension – a numerical-model – application to the Gulf of Lion and Viking Graben. *Earth Planet. Sci. Lett.*, **74**, 92–102.
- MCKENZIE, D. (1978) Some remarks on development of sedimentary basins. *Earth Planet. Sci. Lett.*, **40**, 25–32.
- MJELDE, R., SHIMAMURA, H., KANAZAWA, T., KODAIRA, S., RAUM, T. & SHIOBARA, H. (2003) Crustal lineaments, distribution of lower Crustal Intrusives and structural evolution of the Vøring Margin, Ne Atlantic; new insight from wide-angle seismic models. *Tectonophysics*, **369**, 199–218.
- PRIJAC, C., DOIN, M.P., GAULIER, J.M. & GUILLOCHEAU, F. (2000) Subsidence of the Paris Basin and its bearing on the Late Variscan lithosphere evolution: a comparison between plate and Chablis models. *Tectonophysics*, **323**, 1–38.
- REEMST, P. & CLOETINGH, S. (2000) Polyphase rift evolution of the Vøring Margin (Mid-Norway): constraints from forward Tectonostratigraphic modeling. *Tectonics*, **19**, 225–240.
- REN, S.C., FALEIDE, J.I., ELDHOLM, O., SKOGSEID, J. & GRADSTEIN, F. (2003) Late cretaceous–Paleocene tectonic development of the Nw Vøring Basin. *Mar. Petrol. Geol.*, **20**, 177–206.
- RUPKE, L.H., SCHMALHOLZ, S.M., SCHMID, D.W. & PODLADCHIKOV, Y.Y. (2008) Automated Thermotectonostratigraphic basin reconstruction: Viking Graben case study. *AAPG Bull.*, **92**, 309–326.
- SCLATER, J.G. & CHRISTIE, P.A.F. (1980) Continental stretching: an explanation of the Post-Mid-Cretaceous Subsidence of the Central North Sea Basin. *J. Geophys. Res.*, **85**, 3711–3739.
- SIMON, N.S.C. & PODLADCHIKOV, Y.Y. (2008) The effect of mantle composition on density in the extending Lithosphere. *Earth Planet. Sci. Lett.*, **272**, 148–157.
- SKOGSEID, J. & ELDHOLM, O. (1989) Vøring plateau continental margin: seismic interpretation, Stratigraphy, and Vertical Movements. *Proc. Ocean Drill. Progr., Sci. Res.*, **104**, 993–1030.
- SKOGSEID, J., PLANKE, S., FALEIDE, J.I., PEDERSEN, T., ELDHOLM, O. & NEVERDAL, F. (2000) Ne Atlantic continental rifting and volcanic margin formation. In: *Dynamics of the Norwegian Margin* (Ed. by A. Nottvedt, B.T. Larsen, R.H. Gabrielsen, S. Olaussen, B. Torudbakken, J. Skogseid, H. Brekke & O. Birkeland), *Geol. Soc. Spec. Publ.*, **167**, 295–326.
- STECKLER, M.S. & WATTS, A.B. (1978) Subsidence of Atlantic-type Continental-Margin off New-York. *Earth Planet. Sci. Lett.*, **41**, 1–13.
- SWEENEY, J.J. & BURNHAM, A.K. (1990) Evaluation of a simple-model of Vitrinite reflectance based on chemical-kinetics. *Aapg Bull.-Am. Assoc. Petrol. Geol.*, **74**, 1559–1570.
- TALWANI, M. & ELDHOLM, O. (1972) Continental margin Off Norway – geophysical study. *Geol. Soc. Am. Bull.*, **83**, 3575–3603.
- TERVOORDE, M. & BERTOTTI, G. (1994) Thermal effects of normal faulting during rifted basin formation .1. A finite-difference model. *Tectonophysics*, **240**, 133–144.
- WANGEN, M. (1995) The blanketing effect in sedimentary basins. *Basin Res.*, **7**, 283–298.
- WANGEN, M. & FALEIDE, J.I. (2008) Estimation of crustal thinning by accounting for stretching and thinning of the sedimentary basin – an example from the Vøring Margin, Ne Atlantic. *Tectonophysics*, **457**, 224–238.
- WANGEN, M., FJELDSKAAR, W., FALEIDE, J.I., WILSON, J., ZWIEGEL, J. & AUSTEGARD, A. (2008) Forward modeling of stretching episodes and Paleo Heat Flow of the Vøring Margin, Ne Atlantic. *J. Geodyn.*, **45**, 83–98.
- WATTS, A.B., KARNER, G.D. & STECKLER, M.S. (1982) Lithospheric flexure and the evolution of sedimentary basins. *Philos. Trans. Roy. Soc. Lond. Ser.—Math. Phys. Eng. Sci.*, **305**, 249–281.
- WHITE, N. (1993) Recovery of strain-rate variation from inversion of subsidence data. *Nature*, **366**, 449–452.
- ZHANG, Y.K. (1993) The thermal blanketing effect of sediments on the rate and amount of subsidence in sedimentary basins formed by extension. *Tectonophysics*, **218**, 297–308.

Manuscript received 6 March 2009; Manuscript accepted 26 August 2009